e+i elektrotechnik und informationstechnik

# Preferable PMSM rotor geometry for reduced axial flux components in the stator core

**Norman Blanken · Bernd Ponick**

**Abstract** This paper describes various rotor geometries for the axial end region of permanent magnet synchronous machines (PMSMs) with the aim of reducing the axial magnetic stator flux component. This is achieved by considering the degrees of freedom for the three-dimensional geometry provided by state-of-the-art manufacturing technologies. The comparison of various approaches against conventional arrangements is discussed based on the effects on the axial magnetic stator flux in the end region and on the magnetic flux within the air-gap.

**Keywords** Additive manufacturing · Axial end region · Fringing air-gap flux density · Axial magnetic stator flux · Additional losses

### Bevorzugte PMSM-Rotorgeometrie für reduzierte Axialfluss-Komponenten im Stator

**Zusammenfassung** Dieser Beitrag beschreibt verschiedene Rotorgeometrien für den axialen Endbereich von Permanentmagnet-Synchronmaschinen (PMSMs) mit dem Ziel, den axialen magnetischen Statorflussanteil zu reduzieren. Dies wird durch die Berücksichtigung der Freiheitsgrade für die dreidimensionale Geometrie, die State-of-the-art-Fertigungstechnologien bieten, erreicht. Der Vergleich diverser Ansätze mit konventionellen Varianten wird basierend auf den Auswirkungen auf den axialen magnetischen Statorfluss im Endbereich und auf den magnetischen Fluss im Luftspalt diskutiert.

**Schlüsselwörter** Additive Fertigung · Axialer Endbereich · Ausquellendes Luftspaltfeld · Axialer magnetischer Statorfluss · Zusätzliche Verluste

## Nomenclature

| | |
|---|---|
| $\alpha_{mat}$ | area ratio |
| $\delta$ | air-gap width |
| $\lambda_{ref}$ | magnetic flux coefficient |
| $\mu$ | permeability |
| $\phi_{1,axi}$ | axial magnetic stator flux |
| $\phi_{\delta,A}$ | reduced air-gap magnetic flux |
| $\phi_{\delta}$ | air-gap magnetic flux |
| $\sigma_{axi}$ | axial magnetic stator flux coefficient |
| $A_c$ | curve area |
| $A_r$ | radius area |
| $A_s$ | step area |
| $A_{ch}$ | chamfer area |
| $A_{max}$ | maximum area |
| $h$ | height |
| $k_p$ | packing factor of the laminated stator core |
| $l_1$ | stator length |
| $N_s$ | number of steps |
| $n$ | rotational speed |
| $p$ | number of pole pairs |
| $Q_1$ | number of stator slots |
| $r$ | radius |

## 1 Introduction

Additive manufacturing has the potential to improve the rotors of electrical machines. In terms of lightweight construction, material only needs to be added to the areas of structure where it brings mechanical or electromagnetic benefits. The three-dimensional geometric freedom offered by additive manufacturing enables novel cooling concepts for the rotor, as cooling channels can be arranged in almost

N. Blanken (✉) · B. Ponick
Institute for Drive Systems and Power Electronics, Leibniz University Hannover, Welfengarten 1, 30167 Hannover, Germany
norman.blanken@ial.uni-hannover.de

infinitely complex geometries. In addition, the electromagnetic properties of the rotor in the machine can be influenced by the almost unlimited design possibilities. In [1, 4, 7, 8], some advantages of additive manufacturing are explained with reference to electrical machines.

In electrical machines, magnetic flux does not pass purely radially from the rotor into the stator in the axial end region. Due to the fringing air-gap flux density in this region, a magnetic flux component enters the stator axially [2]. This can lead to additional iron losses, which can be reduced by designing a preferable geometry for the rotor, with this being realised by additive manufacturing. The three-dimensional design freedom offered by additive manufacturing enables the rotor design of an electrical machine to be modified in ways that would not be possible or economically viable with conventional manufacturing techniques. An example longitudinal section through the axial end region of a large cylindrical rotor synchronous machine is shown in Fig. 1. The flux density is illustrated by the size of the vector arrows and by the color gradient. In the middle of Fig. 1, it is shown that a certain portion of the magnetic flux enters the stator axially due to the fringing air-gap flux.

This axial flux contribution to the air-gap field caused by the fringing air-gap flux density is directly related to the geometry of the stator and rotor end regions. The determining parameters are the width of the air gap and the relative lengths of the stator and rotor cores. If the rotor core is longer than the stator core, the axial flux component will increase compared to the case in which both cores are of the same length [3]. Furthermore, when the rotor core is shorter than the stator core, the axial flux entering the stator is reduced[6]. It was shown in [1] that the shape of the axial end region of the rotor has a strong influence on the fringing air-gap flux density and thus on the flux entering the stator axially. Thanks to a radius or a chamfer in the axial end region, the axial magnetic stator flux component could be reduced. However, a design modification in the axial end region must also be investigated concerning its influence on the air-gap magnetic flux $\phi_\delta$. This also allows the influence on the torque to be investigated.
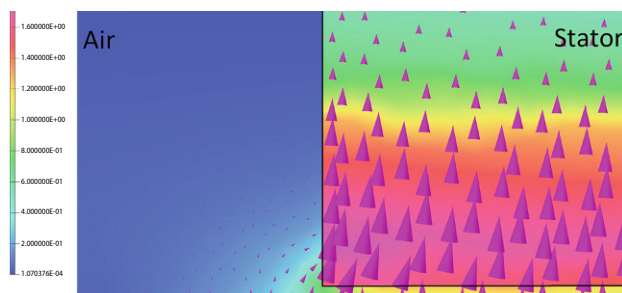
In general, the torque is proportional to the air-gap magnetic flux [5].

In Section 2, design modifications relating to the axial end region which can be realised by additive manufacturing with the aim of reducing the axial magnetic stator flux component are presented. The reference PMSM and the mathematical model for this investigation are described in Section 3. In Section 4, the results of the Finite Element analysis (FEA) concerning the design modifications are presented and evaluated based on their impact on the distribution of the magnetic flux density.
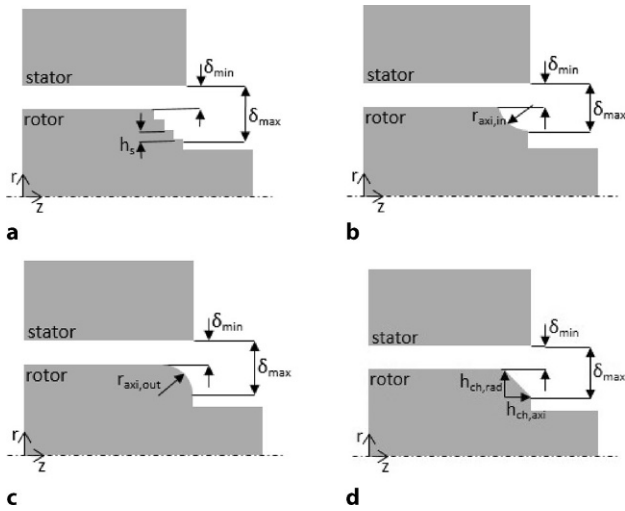
## 2 Design of the axial end region

In large electrical machines, the widening of the air-gap at the ends of the core is realised by gradually increasing the bore diameter of the laminated stator core; this leads to a reduction in flux density and thus to a corresponding reduction in the axial flux components [3]. Figure 2a shows a schematic longitudinal section through the axial end region without any widening of the air-gap and Fig. 2b shows this being realised by gradual widening of the stator. According to [3] and [5], local saturation at the sharp-step edges could be problematic here.

By producing a rotor using additive manufacturing, this approach can be pursued further by widening the air-gap progressively on the rotor side. A gradual reduction of the rotor diameter can be realised by a curve, radius or chamfer. Figure 3b shows the reduction using a curve. This is defined by varying the radius $r_{axi,in}$ and represents a reduction of the area in the axial end region by removing a quarter of a circle from the edge. Figures 3c and d show the same rotor-side widening using a radius or a chamfer, as explained in [1]. The design modification using a radius is defined by varying $r_{axi,out}$ and, using a chamfer, the modification is defined by the height of the chamfer $h_{ch}$. In this paper, $h_{ch,rad}$ is equal to $h_{ch,axi}$, resulting in a 45° chamfer.

Based on the widening of the air-gap in large electrical machines, Fig. 3a shows the widening of the air-gap achieved by a gradual rotor-side stepping. In this paper, variation of the number of steps is investigated. Explicitly square steps were investigated, which



**Fig. 1** Flux density in the axial end region of a cylindrical rotor synchronous machine
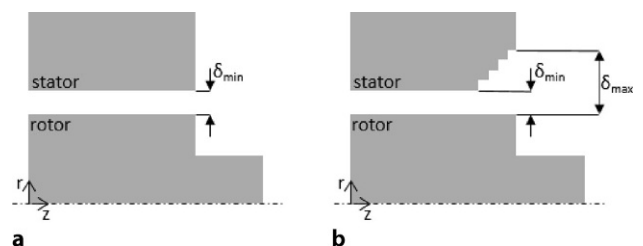


**Fig. 2** Classical widening arrangements in the end region of electrical machines. **a** No air-gap widening, **b** Stator-side gradual widening

**Fig. 3** Schematic longitudinal section through the axial end region of an electrical machine with rotor-side design modifications. Rotor-side widening: **a** steps, **b** curve, **c** radius, **d** chamfer

means that the radial height of all the steps is equal to the axial length of all the steps. This design modification could be produced with conventional manufacturing techniques and should be investigated here as an approach with does not rely upon additive manufacturing.

## 3 Applied methodology

### 3.1 Reference machine

The four design modifications employed in the axial end region are investigated using the rotor of a permanent magnet synchronous machine. The reference machine is an 8-pole synchronous machine with interior permanent magnets in a V-arrangement. Figure 4 shows the cross section of the PMSM concerned. A reference machine with a simple rotor geometry was selected to better allow a focus on the possibilities and design modifications in the axial end region. The rotor, including the shaft, was constructed from one material and designed as a solid model without lamination, as in additive manufacturing. The main data of the machine are listed in Table 1.

In general, the lamination of the stator will prevent the flux from passing through the stator in the axial direction. This is implemented in the FEA by a packing factor $k_p$. This results in anisotropy of permeability in the tangential and normal directions. The modification of the effective permeability in the tangential direction $\mu_t$ and of the effective permeability in the normal direction $\mu_n$ due to the packing factor $k_p$ is determined by

$$\mu_t = k_p\mu_{Fe} + (1 - k_p)\mu_0 \tag{1}$$
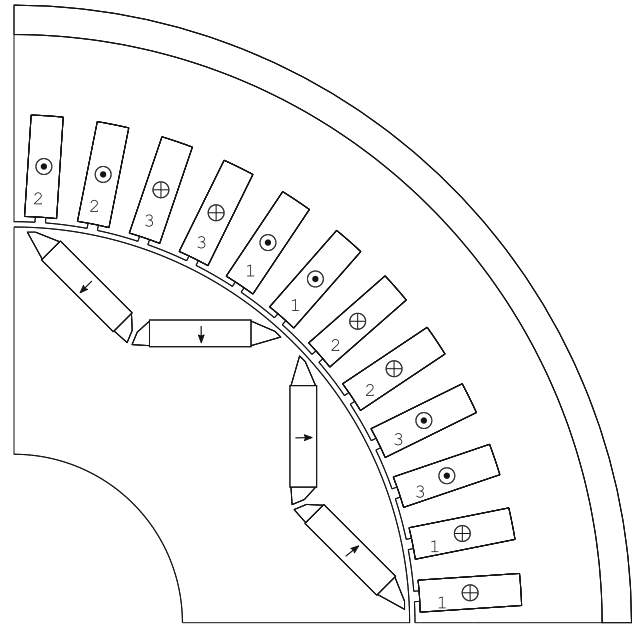


**Fig. 4** Cross section of the reference machine

**Table 1** Data of the reference machine

| number of pole pairs | $p$ | 4 |
|---|---|---|
| number of stator slots | $Q_1$ | 48 |
| stator outer diameter | $D_{a1}$ | 220 mm |
| rotor outer diameter | $D_{a2}$ | 148.5 mm |
| active part length | $l_1$ | 170 mm |
| air-gap length | $\delta$ | 1 mm |
| magnet height | $h_{mag}$ | 5 mm |
| magnet width | $b_{mag}$ | 19 mm |
| edge bridge height | $h_{eb}$ | 1.5 mm |
| rated rotational speed | $n_N$ | 750 min$^{-1}$ |

and

$$\mu_n = \frac{\mu_{Fe}\mu_0}{k_p\mu_0 + (1 - k_p)\mu_{Fe}}, \tag{2}$$

where $\mu_{Fe}$ is the relative permeability of the stator core and $\mu_0$ is the magnetic constant.

### 3.2 Mathematical model

The mathematical model is based on [1] and has been extended to include the step and curve design modifications. The parameters were determined for no-load operation so as to exclude the effect of the stator currents. The axial magnetic stator flux coefficient $\sigma_{axi}$ is determined by

$$\sigma_{axi} = \frac{\phi_{1,axi}}{\phi_\delta}, \tag{3}$$

where $\phi_{1,axi}$ represents the axial magnetic stator flux component and $\phi_\delta$ the total flux passing from the rotor into the stator. The magnetic flux coefficient $\lambda_{ref}$ is determined by

$$\lambda_{\text{ref}} = \frac{\phi_{\delta,\text{A}}}{\phi_{\delta,\text{ref}}}, \tag{4}$$

where $\phi_{\delta,\text{A}}$ represents the total flux passing from the rotor into the stator which has been reduced by the design modifications and $\phi_{\delta,\text{ref}}$ the total flux without design modifications. The area ratio $\alpha_{\text{mat}}$ is determined by

$$\alpha_{\text{mat}} = \frac{A}{A_{\text{max}}}, \tag{5}$$

where $A$ represents the reduced area resulting from the design modifications. The parameter $A_{\text{max}}$ defines the maximum reducible area on the reference machine when the number of steps is equal to one. The maximum step height is limited by the height of the edge bridges so as to avoid modifying the permanent magnets. $\alpha_{\text{mat}} = 0\%$ describes the unchanged reference machine and $\alpha_{\text{mat}} = 100\ \%$ results when $A$ equals $A_{\text{max}}$. The reduced area $A_{\text{s}}$ resulting from a variable number of steps is determined by

$$A_{\text{s}} = \sum_{i=1}^{N_{\text{s}}} i \frac{h_{\text{s}}^2}{N_{\text{s}}^2}, \tag{6}$$

where $N_{\text{s}}$ is the number of steps and $h_{\text{s}}$ is the step height, as shown in Fig. 3a. The radial step height is set equal to the axial step length so as to create square steps. The reduced area $A_{\text{c}}$ resulting from a curve is determined by

$$A_{\text{c}} = \frac{\pi r_{\text{axi,in}}^2}{4}, \tag{7}$$

where $r_{\text{axi,in}}$ represents the variable inner radius of the reduced area, as shown in Fig. 3b. The reduced area $A_{\text{r}}$ resulting from a variable outer radius is determined by

$$A_{\text{r}} = r_{\text{axi,out}}^2 (1 - \frac{\pi}{4}), \tag{8}$$

which reflects the subtraction of the area of a quarter circle from a square with side length $r_{\text{axi,out}}$, as shown in Fig. 3c. The reduced area $A_{\text{ch}}$ resulting from a variable chamfer is determined by

$$A_{\text{ch}} = \frac{h_{\text{ch,rad}} h_{\text{ch,axi}}}{2}, \tag{9}$$

where $h_{\text{ch,rad}}$ is the radial chamfer length and $h_{\text{ch,axi}}$ is the axial chamfer length, as shown in Fig. 3d. In case of a 45-degree chamfer, $h_{\text{ch,rad}}$ equals $h_{\text{ch,axi}}$. In [1], it was shown that the 45-degree chamfer is preferable to a different axial and radial chamfer lengths.

## 4 Results of the Finite Element Analyses

### 4.1 Variation of the number of steps

In Figs. 5, 6 and 7, the results for $\sigma_{\text{axi}}$ are plotted against $\alpha_{\text{mat}}$ while varying the number of steps. In comparison with the maximum $\alpha_{\text{mat}}$, a higher number of steps achieves lower area ratios according to (6). The crosses represent the calculation results from the 3D-FEA. The trend line shows a similar asymptotic behaviour for all numbers of steps. In Figs. 8, 9 and 10, the results for the reduced $\lambda_{\text{ref}}$ are plotted against $\alpha_{\text{mat}}$. Especially at small area ratios, results of the FEA for five steps show an almost constant $\sigma_{\text{axi}}$, but a greatly reduced $\lambda_{\text{ref}}$.

Figures 11 and 12 compare the results for the variation of the number of steps. The trend lines for three and five steps were extended to the theoretical maximum area ratio. The trend line for $\sigma_{\text{axi}}$ shows similar results. The results for one step and for three steps are almost identical. Up to an area ratio of about 50% all trend lines are similar. The trend line for five steps shows an asymptotic course up to $\sigma_{\text{axi}} = 0.52\%$. However, up to an area ratio of 10% the axial magnetic stator flux coefficient is almost constant. The comparison of the results for $\lambda_{\text{ref}}$ shows significant differences. It can be seen that the higher the number of steps, the higher the reduction in the magnetic flux coefficient. Due to the proportionality between the reference flux and the torque, it can be seen from Figs. 11 and 12 that a single step would be preferable.

### 4.2 Variation of the radius of the curve

In Fig. 13, the results for $\sigma_{\text{axi}}$ are plotted against $\alpha_{\text{mat}}$. In comparison with the maximum $\alpha_{\text{mat}}$ and with regard to the height of the edge bridges, the varied radius of the curve achieves a maximum area ratio of about 80% according to (7). The crosses represent the calculation results from the 3D-FEA simulation. The trend line shows an asymptotic course up to $\sigma_{\text{axi}} = 0.51\%$. In Fig. 14, the results for the reduced $\lambda_{\text{ref}}$ are plotted against $\alpha_{\text{mat}}$. The magnetic flux coefficient decreases by 0.11%.

### 4.3 Variation of the radius

In Fig. 15, the results for $\sigma_{\text{axi}}$ are plotted against $\alpha_{\text{mat}}$ for the reference PMSM. In comparison to the maximum $\alpha_{\text{mat}}$ and with regard to the height of the edge bridges, the varied radius achieves a maximum area ratio of about 22% according to (8). The crosses represent the calculation results from the 3D-FEA simulation. The trend line shows an asymptotic course up to $\sigma_{\text{axi}} = 0.56\%$. In Fig. 16, the results for the reduced $\lambda_{\text{ref}}$ are plotted against $\alpha_{\text{mat}}$. As the area ratio increases, the reference flux decreases. However, the influence
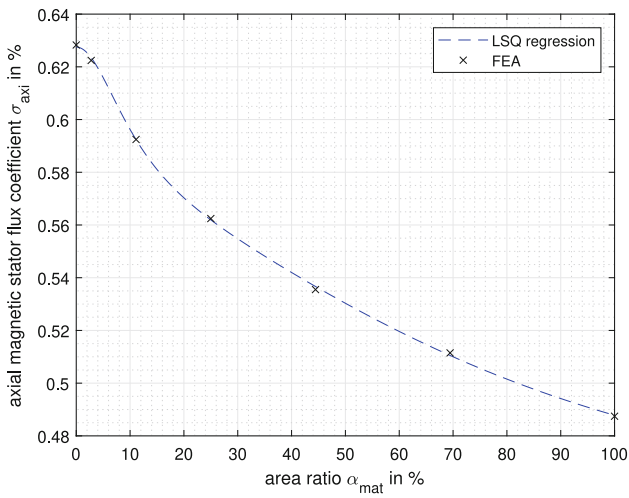
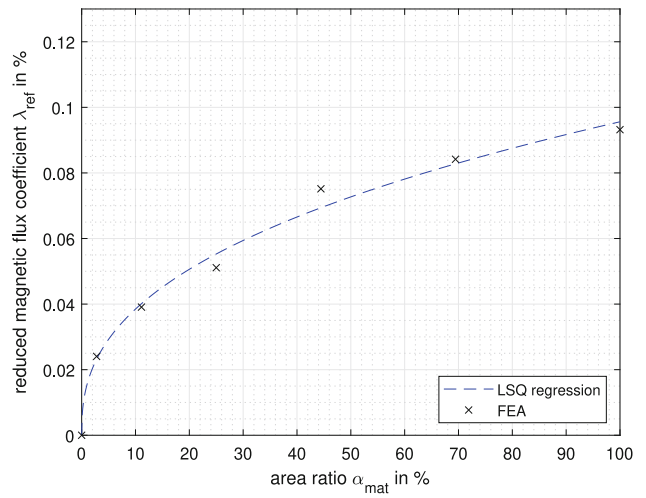**Fig. 5** Axial magnetic stator flux as a function of the area ratio $\sigma_{\mathrm{axi}}(\alpha_{\mathrm{mat}})$ in the case of one step



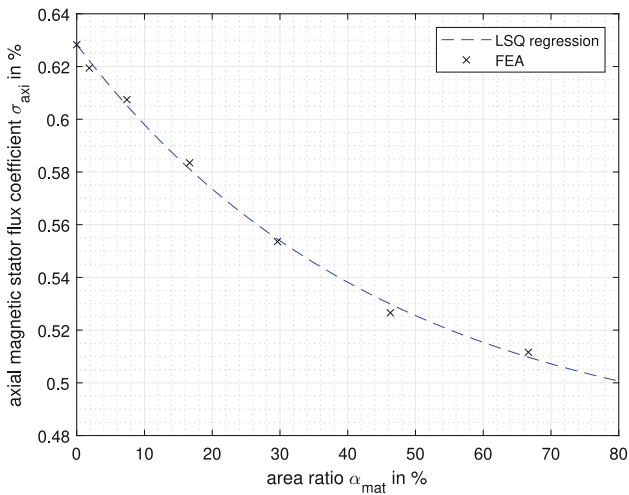**Fig. 8** Reduced magnetic flux as a function of the area ratio $\lambda_{\mathrm{ref}}(\alpha_{\mathrm{mat}})$ in the case of one step



**Fig. 6** Axial magnetic stator flux as a function of the area ratio $\sigma_{\mathrm{axi}}(\alpha_{\mathrm{mat}})$ in the case of three steps
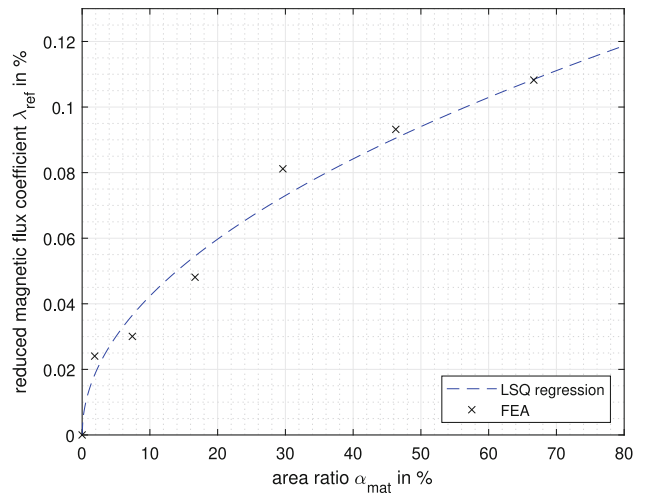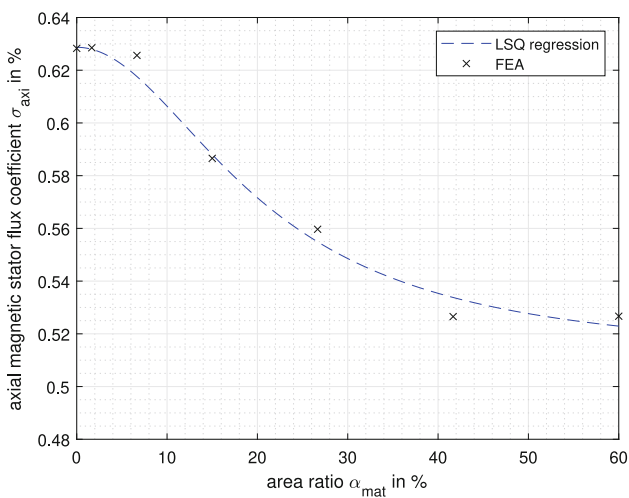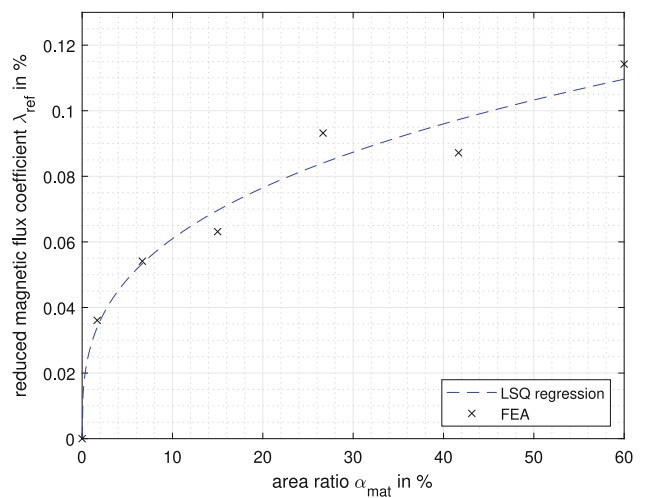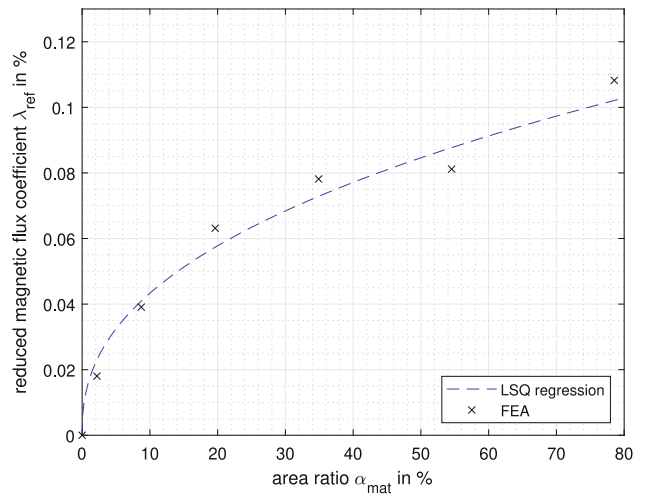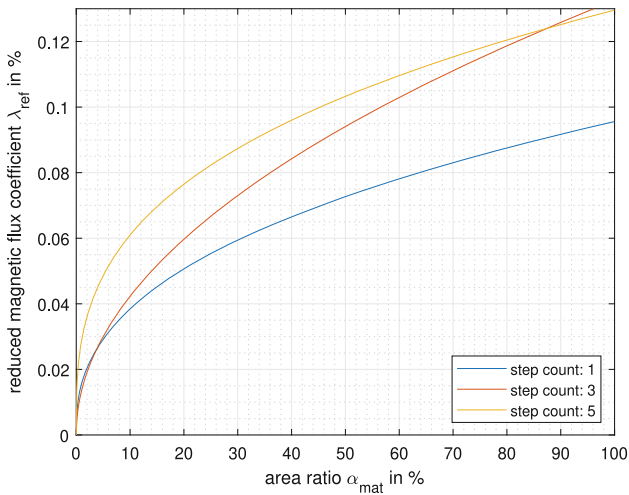


**Fig. 9** Reduced magnetic flux as a function of the area ratio $\lambda_{\mathrm{ref}}(\alpha_{\mathrm{mat}})$ in the case of three steps



**Fig. 7** Axial magnetic stator flux as a function of the area ratio $\sigma_{\mathrm{axi}}(\alpha_{\mathrm{mat}})$ in the case of five steps



**Fig. 10** Reduced magnetic flux as a function of the area ratio $\lambda_{\mathrm{ref}}(\alpha_{\mathrm{mat}})$ in the case of five steps
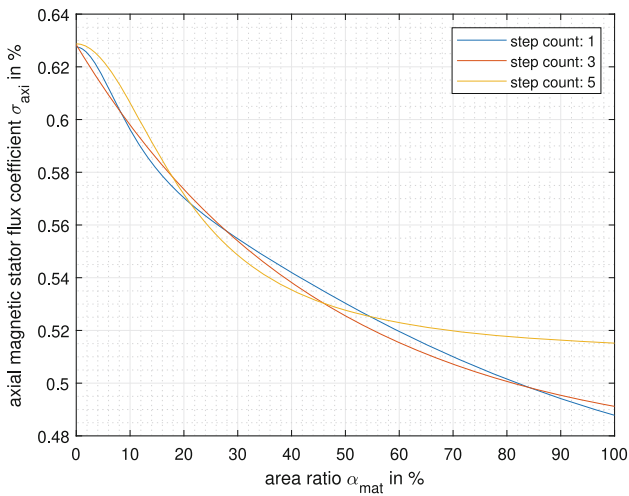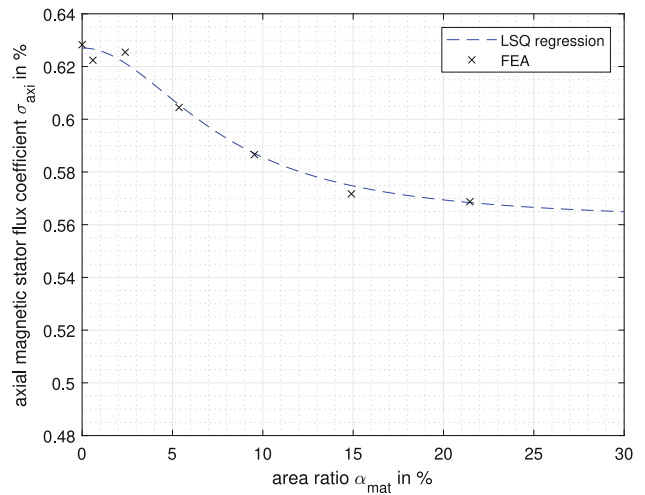
**Fig. 11** Axial magnetic stator flux as a function of the area ratio $\sigma_{axi}(\alpha_{mat})$ in the case of variation of the number of steps
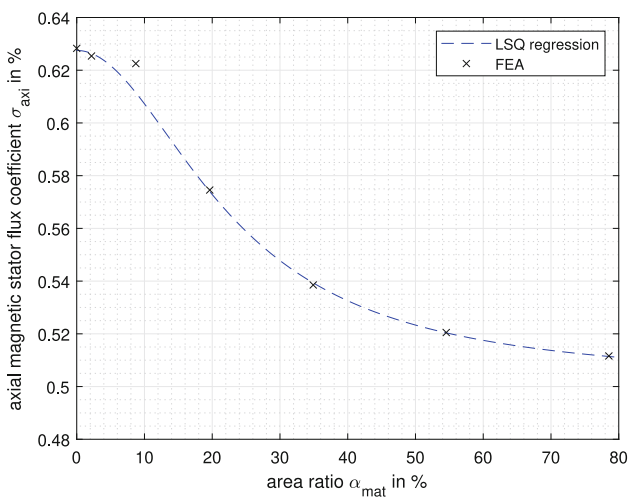


**Fig. 14** Reduced magnetic flux as a function of the area ratio $\lambda_{ref}(\alpha_{mat})$ in the case of a curve
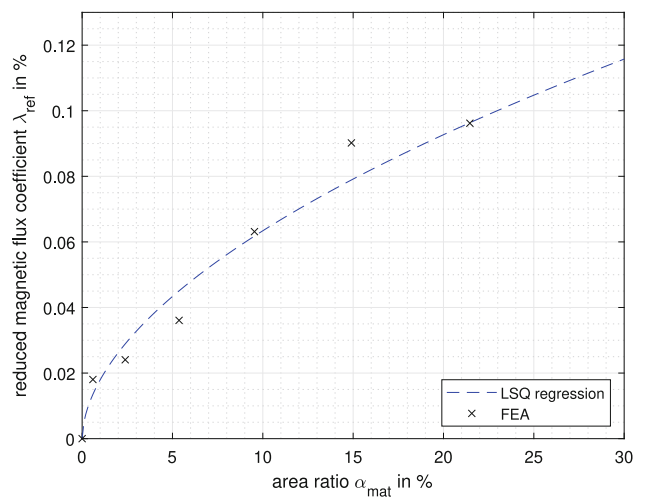


**Fig. 12** Reduced magnetic flux as a function of the area ratio $\lambda_{ref}(\alpha_{mat})$ in the case of variation of the number of steps
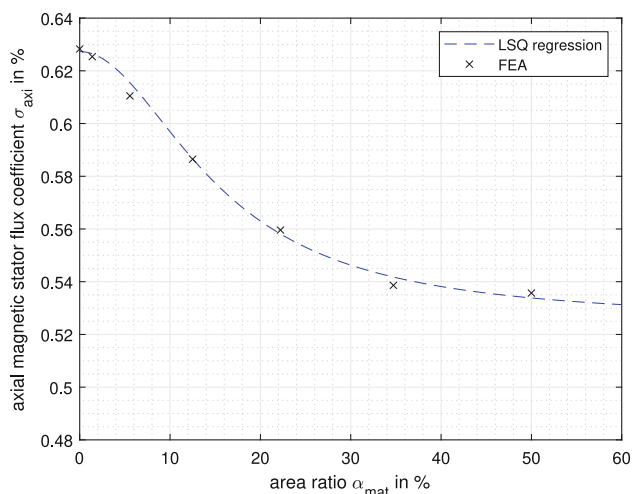


**Fig. 15** Axial magnetic stator flux as a function of the area ratio $\sigma_{axi}(\alpha_{mat})$ in the case of an axial rotor radius
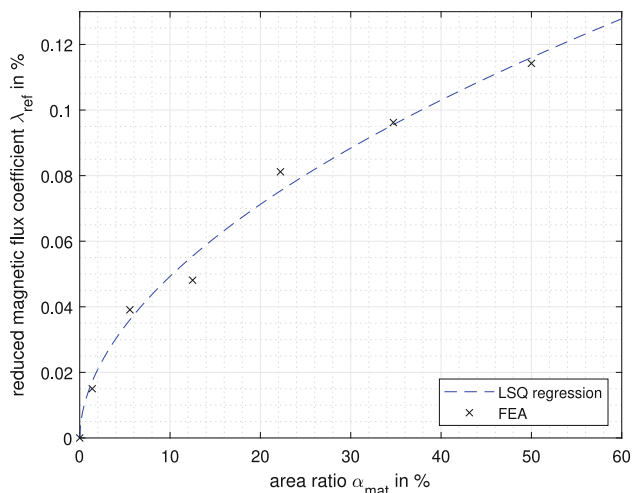


**Fig. 13** Axial magnetic stator flux as a function of the area ratio $\sigma_{axi}(\alpha_{mat})$ in the case of a curve



**Fig. 16** Reduced magnetic flux as a function of the area ratio $\lambda_{ref}(\alpha_{mat})$ in the case of an axial rotor radius

**Fig. 17** Axial magnetic stator flux as a function of the area ratio $\sigma_{\mathrm{axi}}(\alpha_{\mathrm{mat}})$ in the case of a 45° chamfer



**Fig. 19** Axial magnetic stator flux as a function of the area ratio $\sigma_{\mathrm{axi}}(\alpha_{\mathrm{mat}})$



**Fig. 18** Reduced magnetic flux as a function of the area ratio $\lambda_{\mathrm{ref}}(\alpha_{\mathrm{mat}})$ in the case of 45° a chamfer



**Fig. 20** Reduced magnetic flux as a function of the area ratio $\lambda_{\mathrm{ref}}(\alpha_{\mathrm{mat}})$
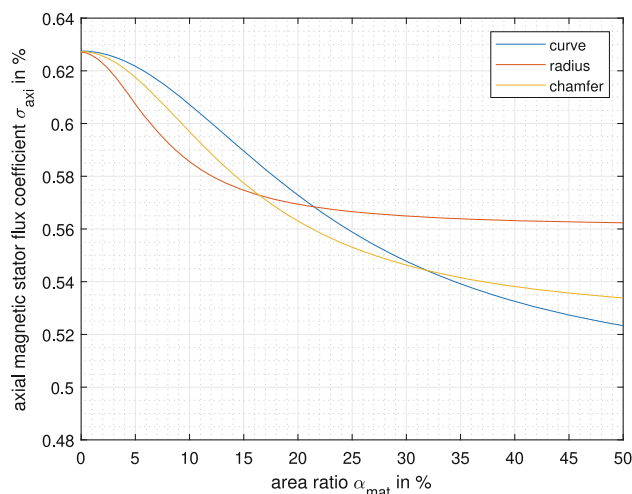
on the reference flux is minimal. The magnetic flux coefficient decreases by 0.11% only.

### 4.4 Variation of the chamfer

In Fig. 17, the results for the design modification using a chamfer for $\sigma_{\mathrm{axi}}$ are plotted against $\alpha_{\mathrm{mat}}$. In comparison with the maximum $\alpha_{\mathrm{mat}}$ and with regard to the height of the edge bridges, the varied chamfer achieves an area ratio of about 50% according to (9). The crosses represent the calculation results from the 3D-FEA simulation. The trend line shows an asymptotic course up to $\sigma_{\mathrm{axi}} = 0.53\%$. In Fig. 18, the results for the reduced $\lambda_{\mathrm{ref}}$ are plotted against $\alpha_{\mathrm{mat}}$. The magnetic flux coefficient decreases by 0.12%.

### 4.5 Comparison of curve, radius and chamfer

Figures 19 and 20 compare the results for the variation of the design modifications without varying the
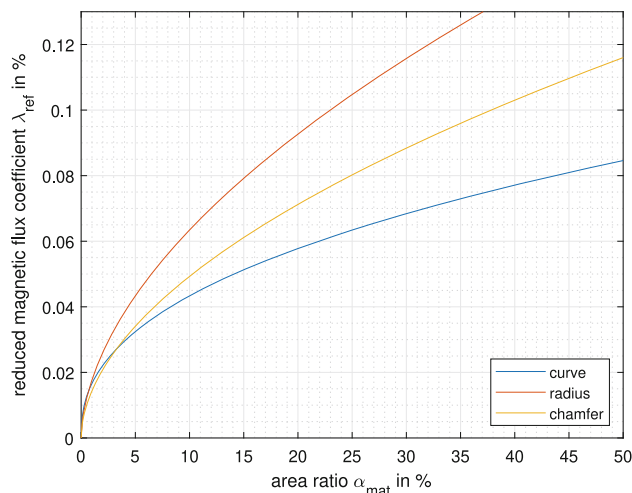
step counts. At small area ratios, the results for the axial magnetic stator flux coefficient obtained using the curve, the chamfer and the radius are similar to the variation of the number of steps. Up to an area ratio of 15%, the radius generates a smaller $\sigma_{\mathrm{axi}}$. Between an area ratio of 15% and 35%, the design modification using a chamfer has a smaller axial magnetic stator flux coefficient. At higher area ratios, the design modification using a curve is the better variant to reduce the axial magnetic stator flux. The comparison of $\lambda_{\mathrm{ref}}$ shows that there are significant differences between the design modifications. Under $\alpha_{\mathrm{mat}} = 5\%$ the trend lines are almost similar. However, the reduction of $\lambda_{\mathrm{ref}}$ caused by the curve is lowest for every area ratio, followed by the design modification using a chamfer. The results for the radius show the greatest reduction in $\lambda_{\mathrm{ref}}$. From this, it can be deduced that, with the design modification using the radius, the torque would decrease the most. However, the reduction in $\lambda_{\mathrm{ref}}$ is very small compared to the reduction in the ax-

ial magnetic stator flux components, and so still fulfills the intention of the design modifications. To make best use of the three design modifications in the reduction of the axial magnetic stator flux components while ensuring a small reduction of the magnetic flux, combinations of these would be possible.

In general, when compared to [1], it can be seen that both, $\sigma_{axi}$ and the reduction of $\lambda_{ref}$, are lower for a PMSM than for a cylindrical rotor synchronous machine. This may be due to the different sizes of the reference machines or the end winding geometry of the field winding.

## 5 Summary and conclusion

In summary, the widening of the air-gap in a PMSM leads to a reduction in the axial magnetic stator flux component. The influence on the reference flux, which is directly related to the torque, is very small. Due to the degrees of freedom for the three-dimensional geometric freedom offered by additive manufacturing, it could be shown in this work that several geometric design variations can yield a reduction in the axial magnetic stator flux component. A comparison to possible conventional manufacturing techniques was conducted by means of investigations with a varying number of steps. It could be shown that the expansion of the air-gap by using a gradual rotor-side widening leads to a reduction in the axial magnetic stator flux component. The comparison of the continuous design geometric modifications in the axial end region shows that there are different ways to reduce the axial magnetic stator flux component. The area ratio determines which of the three design modifications is preferable. For this study, the design modification using a curve showed the best combined results for $\sigma_{axi}$ and $\lambda_{ref}$. Furthermore, the radius showed the best results for smaller area ratios. Additional capabilities are probably given by a combination of the various design modifications.

## 6 Copyright

Figures 1, 2 and 3c,d are subject to IEEE copyright (©2022 IEEE).

## References

1. Blanken N, Bieber M, Ponick B (2022) Design of axial end region of additively manufactured rotors of synchronous machines to reduce the axial magnetic stator flux density. International Conference on Electrical Machines (ICEM), 2022 IEEE, pp 1505–1510
2. Fricke T, Schwarz B, Ponick B (2019) Schwarz-Christoffel-based open-circuit clamping plate field calculation in hydro generators. IEEE International Electric Machines & Drives Conference (IEMDC), 2019 IEEE, pp 1824–1829
3. Howe D, Hammond P (1974) Distribution of axial flux on the stator surfaces at the ends of turbogenerators. Proceedings of the Institution of Electrical Engineers. IET, pp 980–990
4. Ibrahim M, Bernier F, Lamarre JM (2020) Novel multi-layer design and additive manufacturing fabrication of a high power density and efficiency interior pm motor. IEEE Energy Conversion Congress and Exposition (ECCE), 2020 IEEE, pp 3601–3606
5. Müller G, Vogt K, Ponick B (2007) Berechnung elektrischer Maschinen. Wiley-VCH
6. Roshen WA (2007) Fringing field formulas and winding loss due to an air gap. IEEE Trans Magn 43(8):3387–3394
7. Urbanek S (2021) Gestaltung von Rotoren permanent-magneterregter Synchronmaschinen für die Metalladditive Fertigung. TEWISS Verlag, Garbsen/Hannover
8. Urbanek S, Ponick B, Taube A et al (2018) Additive manu-facturing of a soft magnetic rotor active part and shaft for a permanent magnet synchronous machine. IEEE Trans-portation Electrification Conference and Expo (ITEC), 2018 IEEE, pp 668–674

**Norman Blanken,** was born in Bremervoerde, Germany, in 1994. He received the B.Sc. degree and the M.Sc. degree in industrial engineering from Leibniz University Hannover, Hanover, Germany, in 2019 and 2021, respectively. Since 2021, he has been working as a research associate at the Institute for Drive Systems and Power Electronics, Leibniz University Hannover, Hanover, Germany. His research interests include the electrification of aircraft propulsion, the lifetime prediction and predictive mainte-nance of electrical machines.

**Bernd Ponick,** was born in Großburgwedel, Germany, in 1964. He received a Dipl.-Ing. degree in Electrical Power Engineering and a Dr.-Ing. degree in electrical machines, both from the university of Hannover, Germany, in 1990 and 1994, respectively. After nine years in the Large Drives Division of Siemens as a Design Engineer for large variable-speed motors, Head of Electrical Design, and finally as Technical Director of Siemens Dynamowerk Berlin, he now works as Professor for Electrical Machines and Drive Systems at Leibniz University Hannover, a position he has held since 2003. His main research interests include prediction and simulation methods for electrical machines, prediction of and measures to overcome important parasitic effects such as magnetic noise, additional losses or bearing currents, and new applications for electric machines, e.g., for road vehicles or aviation.